Supplemental Information

Contents

S1 BCM learning rule: Why the results of Fig. 1C are general

In Fig. 1C, we showed the behavior of the BCM rule plotted against x, the value of the input activity during MD, and τ_θ/τ_w, the speed of homeostatic plasticity relative to Hebbian plasticity. Here we show that those results are general, independent of assumptions as to the values of the model parameters.

To see this, we transform the variables of the BCM learning rule (Eqs. 1-2). Let $[t]$ denote units of time. If x, y, y_0 and θ all have units of firing rate or $1/[t]$, and w is dimensionless, then for dimensional consistency Eq. 1 should take the form

$$\tau_w \frac{dw}{dt} = kxy(y-\theta) \tag{S1}$$

where k is a constant with units of $[t^3]$. In Eq. 1, we implicitly worked in units in which $k = 1$. Taking the BCM equations to be Eqs. S1 and 2, we define the dimensionless variables $\eta_x \equiv wx/y_0$, $\varphi \equiv \theta/y_0$, $\alpha_x \equiv kx^2 y_0 \tau_\theta/\tau_w$, and $s \equiv t/\tau_\theta$. We have indexed η_x and α_x by x because their values will change when the input activity levels x change, as under MD. In terms of these dimensionless variables we can rewrite the BCM equations as

$$\frac{d\eta_x}{ds} = \alpha_x \eta_x (\eta_x - \varphi) \tag{S2}$$

$$\frac{d\varphi}{ds} = -\varphi + \eta_x^2, \tag{S3}$$

whose unique fixed point is $\eta_x = \varphi = 1$. For a fixed x, the stability of the fixed point depends only on the dimensionless parameter α_x, and the behavior of the model more generally is characterized entirely by α_x and the initial values of η_x and φ at $t = 0$.

We assume that the input activity is x_0 under normal vision and is reduced by a factor of f to $x_{\mathrm{MD}} = f x_0$, $0 < f < 1$, at the onset of MD. We take the initial condition under MD to be the normal-vision fixed point. This initial condition, $\eta_{x_0} = \varphi = 1$, becomes $\eta_{x_{\mathrm{MD}}} = f$, $\varphi = 1$ under MD. Hence, dynamics of this rule under MD are completely characterized by f and $\alpha_{x_{\mathrm{MD}}}$, or equivalently by f and $\alpha_{x_{\mathrm{MD}}}/f^2 = \alpha_{x_0}$. That is, regardless of the choices of the parameters x_0, y_0, k, τ_θ, and τ_w, any models with the same f and α_{x_0} will show exactly the same behaviors of η_{x_0} and φ under normal rearing and of $\eta_{x_{\mathrm{MD}}}$ and φ under MD.

In Fig. 1C, since we took $x_0 = 1$, the y-axis value $x = f x_0$ was equal to f for that model, so the y-axis can more generally taken to be f. Since we also took $k = 1$ and $y_0 = 1$ in that model, the x-axis value τ_θ/τ_w was equal to α_{x_0} for that model, so the x-axis can more generally taken to be α_{x_0}. The illustrated behaviors depend only on f and α_{x_0} and so these plots, with the axes taken to be f and α_{x_0}, are identical for any instantiation of the BCM model regardless of the specific choices of the underlying parameters that give the particular values of α_{x_0}.

In particular, Fig. 1C illustrates w_*, the value of the synaptic strength w at the first trough of synaptic weight under MD relative to its initial value at the onset of MD. From the definition $\eta_{x_{\mathrm{MD}}} = w f x_0/y_0$ and the fact that f, x_0, and y_0 are not changing as MD proceeds, we see that the value at the first trough relative to the initial value is the same for $\eta_{x_{\mathrm{MD}}}$ as it is for w, so the plotted values of w_* vs. f and α_{x_0} are identical for any model. Fig. 1C also illustrates the stability or instability of the MD fixed point, which is determined simply by f and α_{x_0}, and measures the degree of stability by $-\mathrm{Re}\,\lambda\tau_\theta$ where λ is the eigenvalue with largest real part of the BCM equations linearized about the MD fixed point. This stability measure is based on the following: if $\tilde{\lambda}$ is the corresponding eigenvalue of the dimensionless BCM equations, the amplitude of the corresponding eigenvalue develops in time as $e^{\tilde{\lambda}s} = e^{\tilde{\lambda}\frac{t}{\tau_\theta}} = e^{\lambda t}$ where the eigenvalue of the original equation is related to that of the dimensionless equation by $\tilde{\lambda} = \lambda\tau_\theta$. Thus, the stability index is simply $-\mathrm{Re}\,\tilde{\lambda}$, which depends only on f and α_{x_0}.

The BCM rule often includes saturation of Eq. S1 at high y, rather than unlimited, quadratic-in-y growth of $\frac{dw}{dt}$. Therefore it is important to note that our conclusions would not be affected by incorporating such saturation. First, the stability of the fixed point,

$y = wx = \theta = y_0$, is determined by the local properties of Eq. S1 in the vicinity of the fixed point, whereas – to allow sufficient LTP – saturation must occur at values of y well above the fixed-point value. Thus saturation will not affect stability. Next, the value w_* of the synaptic strength at the first trough is invariant to the $y > \theta$ part of Eq. S1 because, starting from the baseline fixed point, the synapse never undergoes LTP until it reaches w_*. Taking these points together, the conclusion of Fig. 1C, that it is impossible to make the adjustment of θ in the BCM rule slow enough to allow realistic closed-eye depression yet fast enough to avoid oscillations or instability, would not be altered by incorporating saturation of Eq. S1 at high y.

S2 Parameter choices for the model that adds stable Hebbian terms and a homeostatic term; Related to Fig. 2

We choose parameters of Eqs. 3–4 to reproduce the results of MD in the monocular cortex (Kaneko et al. 2008b). We choose input activity to be $x = 1$ before MD (and $x < 1$ during MD), and set $w_{\max} = 1$. These choices are arbitrary, setting the scale for the other parameters. The minimum synaptic strength is set to $w_{\min} = 0.6$ because LTD experiments typically depress synapses by ∼30% and, more generally, a few days of MD does not eliminate all synapses. The timescale for plasticity, $\tau_w = 0.3$ day, is chosen so that the synaptic strength reduces to about 70% of the pre-MD value within 3 days of MD in the absence of homeostatic modulation (that is, if $\bar{y}$ is held constant). The timescale for averaging the postsynaptic activity, $\tau_{\bar{y}} = 3$ days, is chosen so that homeostatic plasticity significantly potentiates the synapse after approximately 3 days of MD. Parameters $y_0 = 0.8$ and $\theta = 0.6$ are taken from an appropriate range, within which the results do not significantly change. If $y_0 \ll 1$, then homeostatic plasticity cannot be strong enough to provide sufficient homeostatic potentiation under MD and, at the same time, weak enough to not strongly suppress synaptic strength during normal rearing, which causes synapses to undergo LTD to saturation in the normal condition and thus eliminates MD-induced LTD. If $y_0 > w_{\max}$, then Hebbian and homeostatic plasticity terms are separately zero during normal rearing, which causes a problem when binocular cortex is considered (see discussion below of "condition 1"). If θ is too small, no Hebbian depression happens under a reasonable MD condition, and if θ is too large, the synapse is strongly depressed even under the normal condition. Finally, the magnitude of homeostatic plasticity $\gamma = 0.23$ is chosen so that, after MD and LTD, homeostatic plasticity returns visual response to about 90% of the pre-MD value as in the experimental observations. Larger or smaller γ lead to larger or smaller final weight values, respectively.

While the above discussion suggests that alternative parameters cannot solve the model's problems, we cannot fully explore the parameter space of this model. Nonetheless, we can argue that the conclusions we have reached are general and parameter-independent. These conclusions are: (1) for some ranges of input the Hebbian and system fixed points will not

coincide, meaning that the two forms of plasticity are constitutively active but opposed; (2) where this is true, NMDA blockade should reveal strong weight changes due to homeostatic plasticity; and (3) when the two fixed points are sufficiently far apart, oscillations and/or instability should be seen in the vicinity of the system fixed point. Points (2) and (3) follow from point (1).

The generality of point (1) can be seen from computing the range of input x that allows a fixed point without constitutive plasticity; for the remaining x, any fixed point will have constitutive plasticity. To compute the fixed points, we use $y = wx$ and the fact that at the fixed point $y = \bar{y}$, so that, given w at the fixed point, $\bar{y} = wx$. Fixed points without constitutive plasticity will have $w = y_0/x$ (the condition for no homeostatic plasticity). The condition for no Hebbian plasticity is then either

1. $wx^2 > \theta$ and $w \geq w_{\max}$, *i.e.* $y_0 x > \theta$ and $y_0 \geq w_{\max} x$, or $\theta/y_0 < x \leq y_0/w_{\max}$.
2. $wx^2 < \theta$ and $w \leq w_{\min}$, *i.e.* $y_0 x < \theta$ and $y_0 \leq w_{\min} x$, or $y_0/w_{\min} \leq x < \theta/y_0$.
3. $wx^2 = \theta$, or $y_0 x = \theta$.

For values of x outside of these ranges – that is, for $x > \mathrm{Max}(\theta/y_0, y_0/w_{\min})$, $x < \mathrm{Min}(y_0/w_{\max}, \theta/y_0)$, or $y_0/w_{\max} < x < y_0/w_{\min}$ (the latter condition translates to $w_{\min} < w < w_{\max}$, *i.e.* it is true whenever the fixed-point w is strictly inside the Hebbian bounds) – any fixed point must have constitutive, opposed Hebbian and homeostatic plasticity, *i.e.* the system and Hebbian-only fixed points will not coincide. For example, for the parameters we used in the main text, fixed points will have constitutive plasticity for all values of x *except* $0.75 \leq x \leq 0.8$.

Furthermore, both Hebbian and homeostatic plasticity must be constitutively active at least under the normal rearing condition ($x = 1$) to reproduce ODP. If $x = 1$ satisfies condition 1 or 2, Hebbian plasticity is not active in the normal condition. The summed synaptic strength is determined by the homeostatic constraint $y = y_0$. Then, if we consider inputs from two eyes in binocular cortex, any relative strengths of the two eyes – that is, any ODI – with the given summed synaptic strength will be a fixed point so long as Hebbian plasticity remains saturated for both eyes. But this causes a problem: so long as Hebbian plasticity remains inactive. perturbations of the ODI, *e.g.* due to brief MD, will never recover but will simply persist, which is against experimental observations. In addition, if $x = 1$ satisfies condition 2, there is an additional problem. In this case, Hebbian depression is already saturated during normal rearing. Hence, MD cannot induce further Hebbian depression.

S3 Phase-plane analysis of two models of MD in the monocular cortex; Related to Figs. 2 and 4

Here we use phase-plane analysis to gain an intuition for the reasons that the single-factor model of Eqs. 3-4, which involved Hebbian and homeostatic terms competing to control

changes in w, tended to show weight oscillations. We similarly show in phase-plane analysis why the two-factor model of Eqs. 5-6 does not oscillate, an issue we examine more rigorously in the next section of the Supplemental Information, in which we analyze the stability and origin of oscillations of the model of Eqs. 3-4.

We begin with the single-factor model. The differences in stability of Figs. 2A vs. 2B can be intuitively understood from the phase plane plots of Fig. S1A,B. The arrowed lines show the direction of change in the variables $(w, \bar{y})$ (their time derivatives) for each given value of $(w, \bar{y})$, while line colors indicate the strength of the derivatives, from strongest (blue) to weakest (red). The fixed point of the dynamics, where both derivatives are zero, is given by the intersection of the two black lines: the solid black line represents the locus of points for which $\frac{dw}{dt} = 0$ (the w nullcline), while the dashed black line represents the locus for which $\frac{d\bar{y}}{dt} = 0$ (the $\bar{y}$ nullcline).

The generalized stability of the fixed point, by which we mean whether the fixed point is approached without significant oscillations, is largely determined by the stability of the flow in the w direction (with $\bar{y}$ fixed) at the fixed point: for small perturbations in the w direction from the fixed point, is the w-component of the flow in the opposite direction of the perturbation, back toward the fixed point (stable flow in the w direction) or is it in the same direction of the perturbation, away from the fixed point (unstable flow in the w direction)?

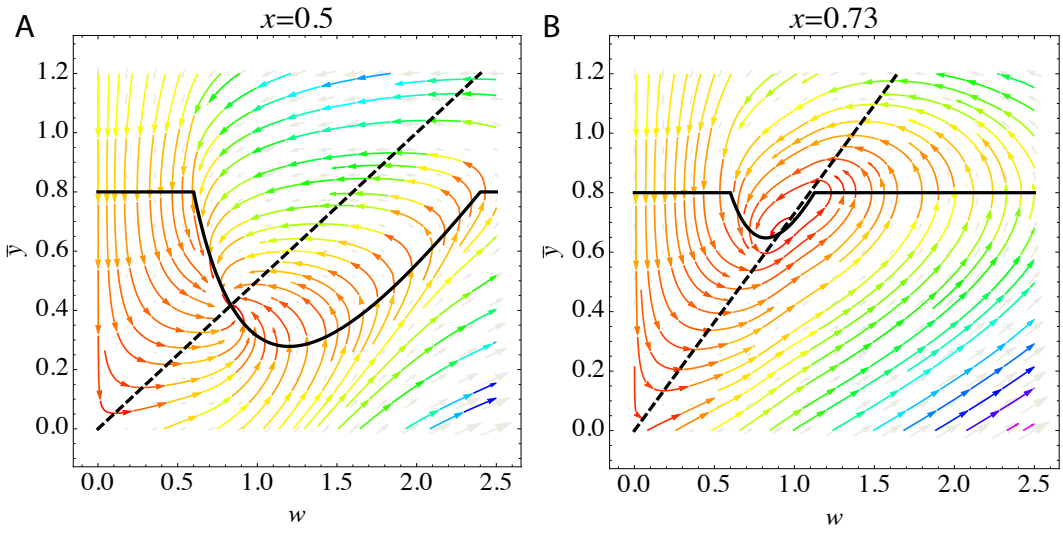

Figure S1: Phase-plane plots of Eqs. 3-4 for $x = 0.5$ (A) and $x = 0.73$ (B). The two axes specify values of averaged postsynaptic activity $\bar{y}$ and synaptic weight w, and the lines with arrows show the direction of change in these two variables from each given point in the plane. The colors of the lines indicate the strength of the derivatives at each point, proceeding red to yellow to green to blue from weakest to strongest. (Strength is assayed as the length of the gradient vector $\frac{dw}{dt}\hat{\mathbf{w}} + \frac{d\bar{y}}{dt}\hat{\bar{\mathbf{y}}}$ where $\hat{\mathbf{w}}$ and $\hat{\bar{\mathbf{y}}}$ are unit-length vectors pointing along the w-axis and $\bar{y}$-axis respectively.) The solid black line shows the w-nullcline (the locus of points along which $\frac{dw}{dt} = 0$) and the dashed line shows the $\bar{y}$-nullcline (the locus of points along which $\frac{d\bar{y}}{dt} = 0$).

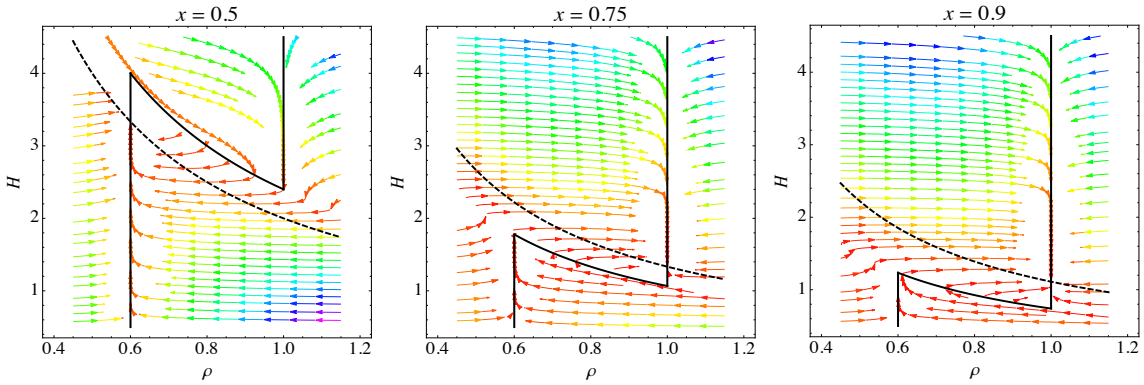

Figure S2: Phase plane analysis of the plasticity model of Eqs. 5-6.
Conventions as in Fig. S1. White regions correspond to regions of very small derivatives.

If the flow is unstable in the w direction, then, because homeostatic plasticity (changes in $\bar{y}$) are slow relative to Hebbian changes, oscillations (or instability) will result: the perturbation will lead to large changes in w before slow changes in y lead to a reversal in the direction of changes in w (a crossing of the w nullcline), which in turn leads to a large change in w in the opposite direction as y slowly changes in the opposite direction, etc. Because the derivative $\frac{dw}{dt}$ is positive below the w nullcline and negative above the w nullcline, the flow in the w direction is unstable if the fixed point is on a positive-sloping portion of the w nullcline, as in Fig. S1B, while it is stable if the fixed point is on a negative-sloping portion of the w nullcline, as in Fig. S1A. The w nullcline transitions from negative to positive slope with increasing w. As x is increased there is a range of x for which the fixed point is found on the positive-sloping region of the w nullcline, leading to oscillations for slow homeostatic plasticity.

In contrast, phase-plane analysis of Eqs. 5-6 (Fig. S2) shows that the fixed point always occurs at one of the two limiting values of ρ, as is clear directly from Eq. 5, and that the flow in the ρ direction is always stable at these limiting values (as is also clear directly from Eq. 5).

S4 Stability of the two-factor, single-synapse model of plasticity; Related to Fig. 4

Here we analytically demonstrate the stability of the fixed point and lack of oscillations in approaching the fixed point of the two-factor, single-synapse plasticity model of Eqs. 5-6. Before more generally analyzing stability, we consider the dynamics in the limit of infinitely slow homeostasis ($\tau_H/\tau_\rho \to \infty$). For simplicity, we set $\tau_\rho = 1$ (which just sets the units of

time), so our equations are

$$\frac{d\rho}{dt} = (\rho_{max} - \rho)[xy - \theta]_+ - (\rho - \rho_{\min})[\theta - xy]_+ \quad \text{(S4)}$$

$$\frac{dH}{dt} = \frac{1}{\tau_H} H(1 - y/y_0) \quad \text{(S5)}$$

with $w = \rho H$ and $y = wx$. Analyzing these equations for $\tau_H \to \infty$ gives an intuitive picture of why, even in the limit of extremely slow homeostasis, there are no oscillations and at most one overshoot of the synaptic weight, as shown in Fig. 5B.

Because of the assumption $\tau_H \to \infty$, we can assume that ρ always moves rapidly (relative to the slow timescale of homeostasis) to a stable fixed point of Eq. S4 for a given value of H, before H changes appreciably. For each H, these stable fixed points of ρ are given by

$$\rho(H) = \begin{cases} \rho_{\max} & \text{when } H > \frac{\theta}{\rho_{\max} x^2} \\ \rho_{\min} & \text{when } H < \frac{\theta}{\rho_{\min} x^2} \end{cases} \quad \text{(S6)}$$

(Fig. S3A). Therefore, the synaptic strength converges rapidly to $\rho(H)H$ (Fig. S3B). Note that $\rho = \rho_{\max}$ and $\rho = \rho_{\min}$ are both stable fixed points when $\frac{\theta}{\rho_{\max} x^2} < H < \frac{\theta}{\rho_{\min} x^2}$, so in this case the choice between these two values of ρ depends on history. Nonetheless, there exists a unique value of H that achieves a particular synaptic strength $w = \rho(H)H$ (Fig. S3B).

The slow change in H can then be described as occuring with ρ always at its stable fixed point, so that $y = wx = \rho(H)Hx$. The dynamics of Eq. S5 can then be written

$$\frac{dH}{dt} = \frac{1}{\tau_H} H[1 - \rho(H)Hx/y_0] \quad \text{(S7)}$$

Thus, H evolves so that $\rho(H)H$ approaches y_0/x ($H = 0$ is an unstable fixed point). Because there is only one value of H that achieves this, the final fixed point is unique and stable. Therefore, even when homeostatic plasticity becomes infinitely slow, there should be no oscillations of weights, but only at most one rapid transition between $\rho_{\max}$ and $\rho_{\min}$, depending on the initial value of ρ, until synapses converge (described further in legend of Fig. S3).

Now, we analyze the stability of the fixed point of Eq. S4 for finite τ_H. Changes in τ_H do not change the locations of the fixed points, but could change their stability. However, since we saw that the fixed points are stable even for $\tau_H \to \infty$, and H provides negative feedback, it would be very surprising if reductions in τ rendered the fixed point unstable, and we will find that this does not happen.

The fixed point depends on the sign of $\phi_0 \equiv xy_0 - \theta$, and is given by: (i) $(\rho, H) = (\rho_{\max}, \frac{y_0}{\rho_{\max} x})$ if $\phi_0 > 0$ and (ii) $(\rho, H) = (\rho_{\min}, \frac{y_0}{\rho_{\min} x})$ if $\phi_0 < 0$. We will prove that the fixed point is stable and without oscillations in either case. Following standard procedures for calculating stability, we consider a small perturbation $\begin{pmatrix} \delta\rho \\ \delta H \end{pmatrix}$ from the fixed point, and consider the linearized dynamics about the fixed point:

$$\frac{d}{dt} \begin{pmatrix} \delta\rho \\ \delta H \end{pmatrix} = J \begin{pmatrix} \delta\rho \\ \delta H \end{pmatrix} \quad \text{(S8)}$$

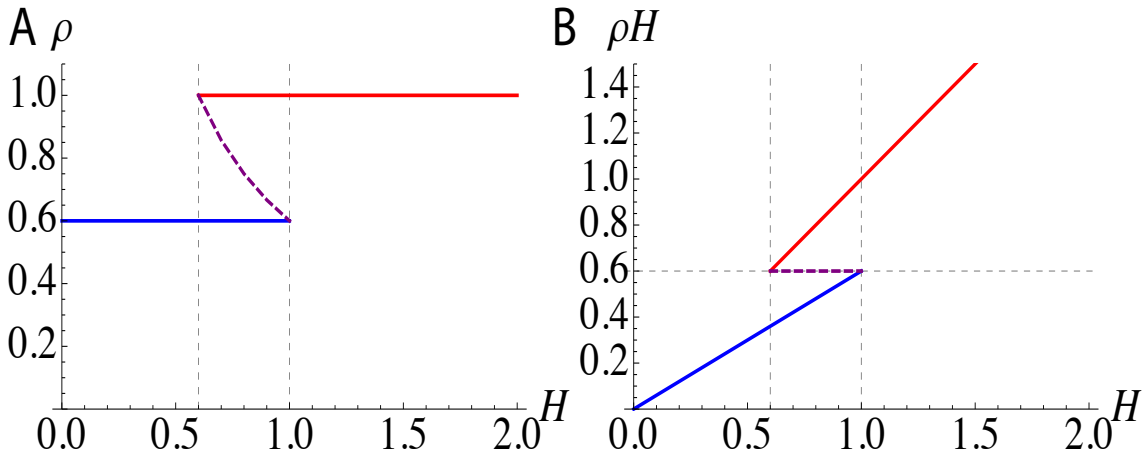

Figure S3: The two-factor model shows at most one overshoot of the synaptic weight before it converges. (A) When the homeostatic plasticity is much slower than Hebbian plasticity, the Hebbian component ρ converges rapidly for each H to its maximum value $\rho_{\max} = 1$ (red line) or minimum value $\rho_{\min} = 0.6$ (blue line). When $\frac{\theta}{\rho_{\max} x^2} < H < \frac{\theta}{\rho_{\min} x^2}$ those two values are bistable and ρ depends on its history. The dashed purple line shows the separatrix (unstable fixed points). (B) The combination of ρ and H that achieves the homeostatic constraint $wx = y_0$, *i.e.* $\rho H = y_0/x$, is unique. Under this dynamics, the synaptic weight ρH moves monotonically along whichever stable branch it starts on toward the stable fixed-point value y_0/x; if this value can only be reached on the other branch, the weight jumps to the other branch (at constant H) when it reaches the end of the first branch, and then evolves monotonically along the second branch to the fixed point. The combination of ρ and H changes accordingly along the stable branches in (A). Thus, there is a monotonic evolution to the fixed point except for possibly one jump between the two branches.

where J is the Jacobian matrix of Eqs. S4-S5 (if r_ρ and r_H are the right-hand sides of Eqs. S4 and S5, respectively, then $J = \begin{pmatrix} \frac{\partial r_\rho}{\partial \rho} & \frac{\partial r_\rho}{\partial H} \\ \frac{\partial r_H}{\partial \rho} & \frac{\partial r_H}{\partial H} \end{pmatrix}$), evaluated at the fixed point. The stability is then determined by the eigenvalues of J. We will find that the eigenvalues are all real, indicating no oscillatory behavior around the fixed point, and negative, indicating stability.

(i) $\rho = \rho_{\max}$ **and** $H = \frac{y_0}{\rho_{\max} x}$ **if** $\phi_0 > 0$**:** In this case the Jacobian matrix is

$$J = \begin{pmatrix} -\phi_0 & 0 \\ -\frac{\gamma y_0}{\rho_{\max}^2 x} & -\gamma \end{pmatrix}, \tag{S9}$$

and the two eigenvalues are $-\phi_0$ and $-\gamma$, which are both negative and real.

(ii) $\rho = \rho_{\min}$ **and** $H = \frac{y_0}{\rho_{\min} x}$ **if** $\phi_0 < 0$**:** In this case the Jacobian matrix is

$$J = \begin{pmatrix} \phi_0 & 0 \\ -\frac{\gamma y_0}{\rho_{\min}^2 x} & -\gamma \end{pmatrix}, \tag{S10}$$

and the two eigenvalues are ϕ_0 and $-\gamma$, which are both negative and real. Hence, the fixed point is stable and shows no oscillatory behavior around the fixed point in either case.

S5 Mathematical relationship between the two factor and conventional model; Related to Figs. 2 and 4-6

In order to better understand this rule and to compare it to the previous rule of Eq. 3, we calculate $\frac{dw}{dt} = H\frac{d\rho}{dt} + \frac{dH}{dt}\rho$.

S5.1 Single-synapse model

We use Eqs. 5-6 to obtain the following mathematically equivalent formulation of the model:

$$\tau_\rho \frac{dw}{dt} = (H\rho_{\max} - w)[xy - \theta]_+ - (w - H\rho_{\min})[\theta - xy]_+ + \frac{\tau_\rho}{\tau_H} w \left(1 - \frac{y}{y_0}\right) \quad \text{(S11)}$$

$$\tau_H \frac{dH}{dt} = H\left(1 - \frac{y}{y_0}\right) \quad \text{(S12)}$$

Equation S11 has a form similar to Eq. 3 and is expressed as a sum of three terms, which correspond to the LTP, LTD, and homeostatic terms of Eq. 3 (with the homeostatic learning speed γ now explicitly represented as $\frac{\tau_\rho}{\tau_H}$). We will refer to the first two terms as the Hebbian terms and the third as the homeostatic term. Note that the factor H that scales the maximal and minimal weights is a postsynaptic-cell-specific factor that is shared across synapses if multiple synapses are considered, while the constants $\rho_{\max}$ and $\rho_{\min}$ might vary from synapse to synapse. The differences between Eq. S11 and Eq. 3 are:

1. The upper and lower limits of the synaptic strength, $H\rho_{\max}$ and $H\rho_{\min}$, are not fixed but are modified by homeostatic plasticity (Eq. S12).

2. The homeostatic term is driven by the instantaneous postsynaptic firing rate as opposed to the running-average of the postsynaptic firing rate in Eq. 3. Thus, there is no delay in the homeostatic term; as we have seen, delays can cause oscillations of synaptic strength.

3. A minor difference is that Eq. S11 uses linear functions $(H\rho_{\max} - w)$ and $(w - H\rho_{\min})$, whereas Eq. 3 uses threshold-linear functions $[w_{\max} - w]_+$ and $[w - w_{\min}]_+$. Thresholding would not alter the dynamics in Eq. S11 because the synaptic weight under Eqs. S11-S12 is always restricted to $H\rho_{\min} \leq w \leq H\rho_{\max}$. This may not be obvious under Eqs. S11-S12, but is obvious from the equivalent Eqs. 5-6 and the relationship $w = \rho H$.

Thus, our proposed model can equivalently be understood as one in which Hebbian and slow-but-instantaneous homeostatic plasticity both compete to modify w, but in addition homeostatic plasticity continually modifies the minimal and maximal weight values. With

homeostatic modification of limiting weight values, the Hebbian terms in Eq. S11 approach a stable state of zero plasticity with weights saturated at their limiting values, and this state remain undisturbed as homeostatic plasticity proceeds until it too reaches zero. For this reason, Eqs. S11-S12 generically reach a steady state in which there is no constitutive plasticity (*i.e.*, Hebbian and homeostatic plasticity are each separately zero), as is perhaps more obvious from the equivalent Eqs. 5-6, whereas the seemingly very similar Eq. 3 generically reaches a steady state in which Hebbian and homeostatic plasticity are each constitutively active but opposed (*i.e.* their sum is zero, but the terms individually are not zero).

S5.2 Multi-synapse model

We now use Eqs. 7-9 to compute $\frac{dw}{dt}$. We define the step function $\Theta(x)$ by $\Theta(x) = 0$, $x \leq 0$; $\Theta(x) = 1$, $x > 0$. Note that parameters $\rho_{\max}$ and $\rho_{\min}$ may vary across synapses though we do not make this explicit here. Then our equations become[1]

$$\begin{aligned} \tau_\rho \frac{dw_i}{dt} &= (H\rho_{\max} - w_i)[\phi_i]_+ - (w_i - \sqrt{H}\rho_{\min})[-\phi_i]_+ \\ &\quad + \Theta(H-1)\frac{\tau_\rho}{\tau_h} w_i \left(-1 + \frac{1}{H} F\left(\frac{Hy_0}{\langle y \rangle}\right)\right) \qquad \text{(S13)} \\ H &= \text{Max}(h, 1) \qquad \text{(S14)} \\ \tau_h \frac{dh}{dt} &= -h + F\left(\frac{Hy_0}{\langle y \rangle}\right) \qquad \text{(S15)} \end{aligned}$$

Equation S13, like Eq. S11, is the sum of an LTP, an LTD, and a homeostatic term. Equation S13 is more complex than Eq. S11 for two reasons: the H-dependence of $\rho_{\min}$ manifests as a $\sqrt{H}$ rather than H scaling of the minimum weight (with the understanding that $H \geq 1$, Eq. S14); and the dependence of H on h manifests as the complex homeostatic plasticity term. Despite this complexity, Eq. S13 has the same three properties as we described above for Eq. S11. Thus, the multi-synapse model can again be equivalently understood as one in which Hebbian and slow-but-instantaneous homeostatic plasticity both compete to modify w, but in addition homeostatic plasticity continually modifies the minimal and maximal weight values. This again leads to a steady state in which Hebbian and homeostatic plasticity are each separately zero (no constitutive plasticity), for the same reasons just outlined for the single-synapse model.

S6 Parameter dependency of the simple two factor model; Related to Fig. 4C

In Fig. 5C, we considered relatively strong deprivation, $x = 0.5$, applied for 5 days. Here, we considered a weaker deprivation, $x = 0.75$, maintained for a long period (Fig. S4A). This led

[1]We neglect the fact that the homeostatic term in Eq. S13 is also nonzero if $H = h = 1$ and $\frac{dh}{dt} > 0$. This condition holds only for an infinitesimal amount of time and hence contributes negligibly to Eq. S13.

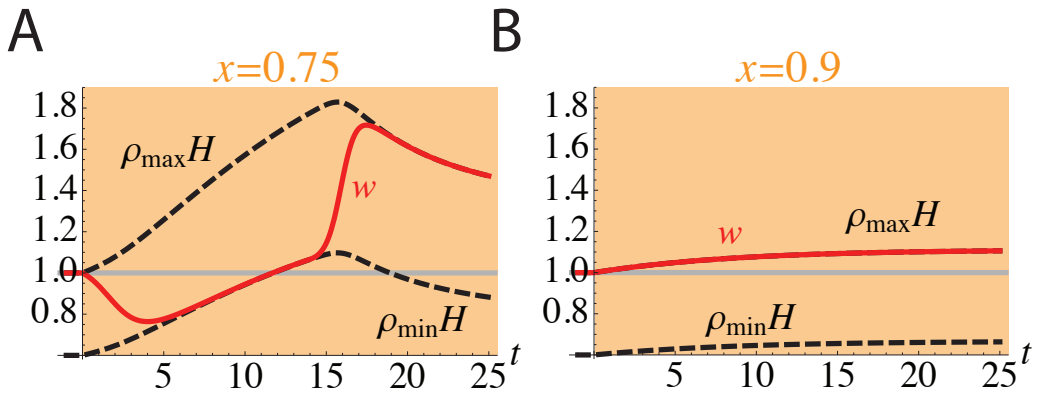

Figure S4: Simulation results of the two-factor model in the monocular cortex during mild MD. The conventions are as in Fig. 4C but input is stronger during MD. (A) For intermediate input activity during MD, the weight was depressed by Hebbian plasticity to the minimum strength, but in this case the slow homeostatic potentiation during continued MD ultimately brought the pre- and postsynaptic correlation $xy = wx^2$ above the LTP threshold θ. This induced LTP to the maximum synaptic value, followed by slow homeostatic decrease of this maximum value. (B) For large input activity during MD, there was no LTD. The synaptic strength remained at the maximal value and homeostatic plasticity slowly increased the maximal value to compensate for the slight loss of input.

to a similar trajectory of initial LTD followed by slow homeostatic scaling up of the weights. However, when we allowed the deprivation to continue for an extended period, the scaling brought the synaptic strength across the LTP/LTD threshold. At that point, just as in the case of recovery in Fig. 5C, rapid LTP increased ρ until it reached its maximal value, after which homeostatic plasticity slowly reduced the synaptic strength.

Next, we considered still weaker deprivation, $x = 0.9$ (Fig. S4B). In this case, the decrease in the input firing rate was small enough that the LTP/LTD threshold was not crossed, so there was no initial LTD and ρ remained at $\rho_{\max}$. Homeostatic plasticity slowly compensated for the reduction of the input by potentiating the synapse.

The strongest deprivation robustly yields the behavior we are seeking to explain: fast LTD followed by slow homeostatic compensation (Fig. 5C). For weaker deprivation, alternative behaviors are seen. The overshoot of synaptic strength after long periods of intermediate-strength deprivation (Fig. S4A) depends on homeostasis strengthening synapses sufficiently to cross the Hebbian LTD/LTP threshold, and this in turn depends on model details. It would not occur, for example, if an appropriate maximum value were imposed on H. Homeostatic strengthening in response to mild deprivation (Fig. S4B) might accurately describe the homeostatic strengthening of excitatory synapses in response to visual deprivation that occurs in layer 4 of rat visual cortex before the opening of the critical period for MD-induced ODP (Maffei et al. 2004). Before the opening of the critical period, visually-driven activity is likely to be weak relative to spontaneous activity (Toyoizumi et al. 2013), so that the

effects of deprivation on cortical activity may be relatively weak.

S7 Model modifications for the multi-synapse model; Related to Figs. 5 and 6

S7.1 Modification of the homeostatic and Hebbian rules

For the multi-synapse plasticity models, we used a more complicated homeostatic rule than the simpler rule of Eq. 6, and incorporated H-dependence of $\rho_{\min}$ into the Hebbian rule, to try to solve several problems of the simpler rule:

- There is continued ODP towards the open eye during 3-7 days of MD that is TNF-α dependent (it does not occur in TNF-α KO animals nor in animals in which TNF-α receptors are blocked) (Kaneko et al. 2008b). To model this effect, we incorporated a reduction of $\rho_{\min}$ with increases of the homeostatic variable H, so that increases of H allowed further LTD. The dependence on H should be weaker than a $1/H$ dependence because, otherwise, homeostatic scaling could not potentiate synapses in a depressed state.

  Other factors could also contribute to TNF-α-dependent ODP, but we restricted to a single factor for simplicity. These other factors include: (1) a similar increase in $\rho_{\max}$ with increasing H could allow TNF-α-dependent LTP of the open eye; (2) there could be a minimal, threshold level of pre-post covariance for inducing LTD, so that LTD stops at an intermediate weight level initially as LTD lowers the covariance, but resumes as TNF-α-dependent homeostatic plasticity increases the covariance; (3) Better representation of the stochasticity of neural activity and plasticity should allow a broader distribution of synaptic strengths in the normal state. Then, after 3 days of MD, a larger percentage of open-eye synapses would be in the LTD state than in our model despite an overall shift toward LTP, and similarly a larger percentage of closed-eye synapses would be in the LTP state despite a shift toward LTD. Homeostatic strengthening of response might lead Hebbian plasticity to squeeze these distributions, adding to TNF-α-dependent LTP of the open eye and LTD of the closed eye. (Note that factors like stochastic broadening of the synaptic distribution and/or a minimal covariance threshold for LTD are also necessary to explain why LTP and LTD protocols work, e.g. why in the normal state all synapses are not already saturated at the potentiated state before the protocol is applied, assuming that individual synapses are generally saturated (O'Connor et al. 2005, Petersen et al. 1998). Note also that our model fails to quantitatively account for the strength of decrease in open-eye potentiation induced by NMDA blockade. This could be fixed by factors (1) or (3) above or by further modifications of the homeostatic rule, but we neglected this for simplicity.)

- In the simple rule, homeostatic plasticity, while slow, was active from the initiation of MD. As a result, significant homeostatic plasticity had already occurred at the

time of maximal LTD (evident as the rise of $\rho_{\min}H$ by day 2 in Fig. 4C). While this caused no problem for the single-synapse model of monocular cortex studied previously, in a binocular cortex model this would mean that some potentiation of open-eye responses would already be visible at that time, unlike experiments (Kaneko et al. 2008b). This might be explained by LTD of the open eye that offsets homeostatic potentiation, but this is unlikely because no depression of open eye responses is observed in TNF-α knockout mice (Kaneko et al. 2008b). To explain this, we assumed a more complex homeostatic rule that delays the onset of homeostatic plasticity until a threshold amount of an underlying factor is accumulated. Other factors we did not consider, such as necessity of a threshold amount of activity deviation from the set point before homeostatic plasticity begins, could also or alternatively be involved.

- Stellwagen and Malenka (2006) showed that TNF-α signaling is required for scaling up of synaptic weights in response to activity blockade, but not for scaling down of synaptic weights in response to excess activity induced by inhibitory blockade. To capture this, we modified the rule so that H can increase from a baseline level of 1 (representing scaling up from baseline) but cannot decrease below 1 (meaning that scaling down from baseline is not achieved by modification of H).

- Homeostatic plasticity does not appear to perfectly compensate for activity changes. The homeostatic increase seems to be a scaling up of about 30% from the level at day 3, both in monocular and binocular cortex, which in monocular cortex restores synaptic weights to near the pre-MD level (Kaneko et al. 2008b); this would not be sufficient to restore activity to its pre-MD level under continuing MD. To match this, we made the growth of H a saturating function of the ratio of actual to set-point activity, preventing full compensation for the activity decrease. This could also be explained by a lack of activation of homeostatic plasticity by activity deviations from the set point of less than a threshold amount.

To capture these ideas, we assumed the more complex homeostatic rule of Eqs. 8–9. In Eq. 9, $F(x)$ (Eq. S16) is a monotonically increasing function that is 0 for $x \leq 1$, jumps from 0 to 1 when x exceeds 1 and then increases roughly linearly with x until it saturates at around 2. The mathematical form used was

$$F(x) = [1 + \tanh(x - 1)]\Theta(x - 1.01) \tag{S16}$$

where $\Theta(z)$ is a step function, $\Theta(z) = 1$ for $z \geq 0$, $= 0$ otherwise. The shape of this function is illustrated in Fig. S5A. The argument of F is chosen to be $Hy_0/\langle y\rangle$ so that, if F did not saturate (*e.g.*, if $F(x) = x$), the stable fixed point of homeostatic plasticity, starting from a condition with $y_0/\langle y\rangle > 1$, would be $\langle y\rangle = y_0$. That is, the homeostatic rule restores the set-point activity for smaller decreases of activity, but saturation prevents full restoration for larger decreases of activity.

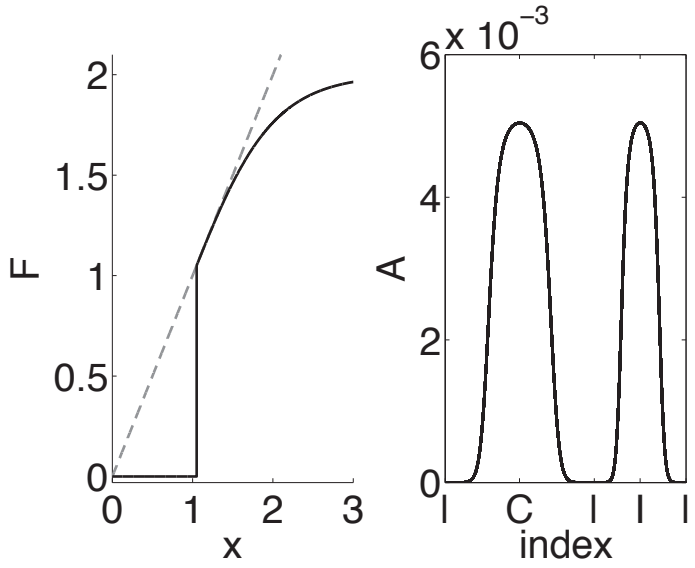

Figure S5: (A) The nonlinear function F used in Eq. 8 to update h. This function is monotonically increasing, jumping from 0 to 1 at $x \approx 1$ and then smoothly saturating at around 2. (B) The arbor function A used in the multi-synapse plasticity models for binocular cortex in the expression for synaptic strength $w_i = HA_i\rho_i$. The value of A_i (Eq. S17) is shown vs. index value i, where indices $i = 1, \ldots, 310$ are from the closed eye (contralateral eye, labeled 'C') and $i = 311, \ldots, 500$ are from the open eye (ipsilateral eye, 'I').

S7.2 The arbor function

The axonal arborization function A_i describes the anatomical density of axon branches to the postsynaptic neuron from a given presynaptic neuron i. The arborization strengths are given by

$$A_i \propto \frac{1}{1 + \exp(3[(z_i - 0.5)^2/(0.2)^2 - 1])}, \tag{S17}$$

where the overall strengths are normalized according to $\sum_{i=1}^{N} A_i = 1$. The shape of this function is illustrated in Fig. S5B for the binocular case and in Fig. S6C for the monocular case.

S8 MD results of the two-factor, multi-input model in the monocular cortex; Related to Fig. 5

Here we examine the results of MD in monocular cortex for the multi-input model of Eqs. 7-9 (Fig. S6). MD to the contralateral eye was started at day 0 and the eye was re-opened at day 7. Initial LTD induced rapid decrease of the Hebbian factors, ρ, and homeostatic potentiation was induced by the delayed increase of the homeostatic factor H. Homeostatic

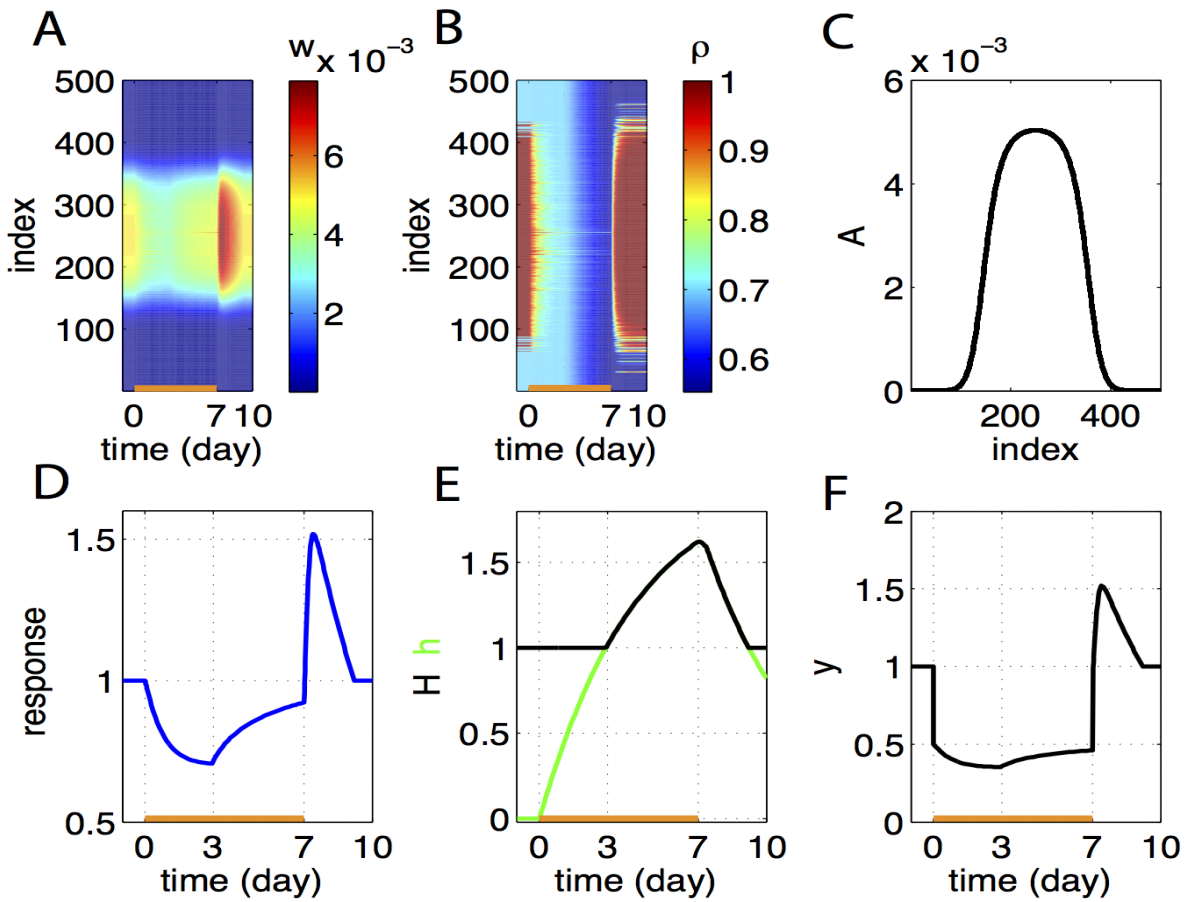

Figure S6: Simulation result in the monocular cortex before, during, and after MD using the model of Eqs. 7-9. We considered 500 inputs from the contralateral eye, which was closed during MD. MD was started at day 0 and the closed eye was re-opened at day 7. (A) Synaptic strengths w_i are shown as a function of developmental time. (B) The Hebbian factors ρ_i. (C) The arbor function A_i. (D) The normalized visual response (defined as in Fig. 5). (E) The homeostatic factor H (black) and h (green). (F) The average postsynaptic firing rate $\langle y \rangle$.

plasticity was absent for the first few days of MD because it took time for h to reach the threshold value of 1. After the re-opening of the contralateral eye, the model showed an overshoot of synaptic strengths (Fig. S6A,D), as in the single-synapse model of monocular cortex and in the multi-input model of binocular cortex. As in those cases, this behavior occurred because, after restoring normal visual input, the Hebbian component ρ potentiated rapidly and the homeostatic factor H more slowly decayed back to its baseline.

S9 Experimental Methods; Related to Figs. 3 and 7

In vivo experiments: C57BL/6 wild type breeders were purchased from Charles River Laboratories (Hollister, CA) and bred as needed. Animals were maintained in the animal

facility at University of California San Francisco and used in accordance with protocols approved by the UCSF institutional Animal Care and Use Committee. Total of 47 C57BL6 male mice were included for the analysis.

Monocular deprivation (MD) was performed by suturing shut the right eyelid (contralateral to the imaged hemisphere) at P25 as described (Kaneko et al. 2008b). The initial day of imaging was described as day 0 and other days are numbered sequentially from there. To produce recovery from effects of MD, vision was restored to the closed eye by simply removing the suture. All mice were kept under standard housing conditions with free access to food and water between recordings.

NMDA blockade: Two days prior to recording baseline responses, a custom stainless steel plate for head fixation was attached to the skull with dental acrylic under isoflurane anesthesia as described (Kaneko and Styker, 2014). Animals were given a subcutaneous injection of carprofen (5 mg/kg) as a post-operative analgesic. The competitive NMDA receptor antagonist (R,S)-3-(2-carboxypiperazin-4-yl)propyl-1-phosphonic acid (CPP) (Tocris Bioscience) was dissolved in saline at a concentration of 1 mg/ml and the drug solution was injected intraperitoneally at a dose of 15 mg/kg roughly every 24 h, as described (Sato and Stryker 2008). The first injection in each experiment was performed right after the imaging of the corresponding day. On subsequent days, injections were made around 9AM, and imaging, if done, occurred 1-6 hours after injection (1 hr for the first mouse imaged, 6 hr for the last mouse imaged on given day). As expected, baseline response levels were indistinguishable in CPP and control animals (Fig. S7).

TNF-α blockade: Intracortical infusion of soluble TNF receptor-1 (sTNFR1, R&D Systems, Inc. Minneapolis, MN) was performed as described (Kaneko et al. 2008b, except that implantation was done on day 0). Briefly, on day 0, immediately after baseline imaging, we implanted a cortical cannula that was connected with an Alzet osmotic minipump (model 1002) filled either with vehicle solution (PBS containing 0.1% bovine serum albumin as a carrier) or 35 mg/ml of sTNFR1. This was followed immediately by eyelid suture. Infusion continued during days 0-5 of 6-day MD. On day 5, the cannula and minipump were removed and response magnitudes (MD-5d) were then recorded. On day 6, vision was restored to the closed eye by simply removing the suture to produce recovery from effects of MD, and responses were recorded 24 and 48 hours after reopening the closed eye.

Repeated optical imaging of intrinsic signals and quantification of ocular dominance were performed as described (Kaneko et al. 2008a). Briefly, during recording mice were anesthetized with 0.7% isoflurane in oxygen applied via a home-made nose mask, supplemented with a single intramuscular injection of 20-25 g chlorprothixene. Intrinsic signal images were obtained with a Dalsa 1M30 CCD camera (Dalsa, Waterloo, Canada) with a 135x50 mm tandem lens (Nikon Inc., Melville, NY) and red interference filter (610 $\pm$ 10 nm). Frames were acquired at a rate of 30 fps, temporally binned by 4 frames, and stored as 512x512 pixel images after binning the 1024x1024 camera pixels by 2x2 pixels spatially. The visual stimulus for recording in the binocular zone, presented on a 40x30 cm monitor placed 25 cm in front of the mouse, consisted of 20^0-wide bars, which were presented between -5^0 and 15^0 on the stimulus monitor (0^0 = center of the monitor aligned to center of the mouse) and moved

Figure 3B with the absolute levels of response

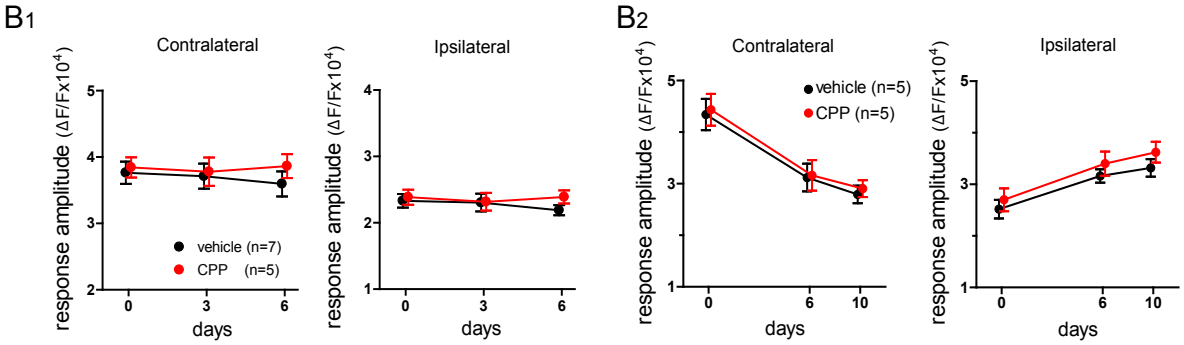

Figure 7A with the absolute levels of response

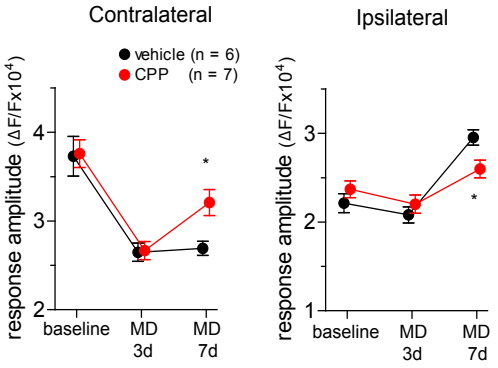

Figure S7: The CPP results in Figs. 3B and 7A remain identical when the results are shown in terms of the absolute amplitude of visual response ($\Delta F/F * 10^4$). Conventions as in Figs. 3B and 7A.

continuously and periodically upward or downward at a speed of 10^0/sec. The phase and amplitude of cortical responses at the stimulus frequency were extracted by Fourier analysis as described (Kalatsky and Stryker, 2003). Ocular dominance index (ODI) was computed as $(R-L)/(R+L)$, where R and L are the peak response amplitudes through the right eye and the left eye, respectively, as described (Kaneko et al. 2008a). Response amplitude at each time point in individual animals was an average of at least 4 measurements.

Statistical analyses: For changes after monocular deprivation or recovery from deprivation, the response magnitude in individual animals was normalized to the baseline magnitude, followed by calculating group average and S.E.M. Response magnitudes and ocular dominance index data were analyzed by a two-way ANOVA to determine the effects of pharmacological treatments (CPP or sTNFR1) and of manipulations of visual experiences (ND, MD, or binocular recovery) in Prism 6 (GraphPad Software, CA). For multiple comparisons, Bonferroni corrections were used.

Supplemental References:

Kaneko, M., and Styker, M.P. (2014) Sensory experience during locomotion promotes recovery of function in adult visual cortex. eLife, e02798.

Maffei, A., Nelson, S. B., and Turrigiano, G. G. (2004) Selective reconfiguration of layer 4 visual cortical circuitry by visual deprivation. Nature Neurosci., 7(12):1353-1359.

Sato, M., and Stryker, M.P. (2008). Distinctive features of adult ocular dominance plasticity. J. Neurosci. 28, 7520-7536.

Kalatsky, V.A., and Stryker, M.P. (2003) New paradigm for optical imaging: temporally encoded maps of intrinsic signal. Neuron 38, 529-545.